Astron. Astrophys. 281, 871–881 (1994)

ASTRONOMY AND ASTROPHYSICS

Very Long Baseline Interferometry of 1720 MHz masers in W3(OH)

M.R.W. Masheder[1], **D. Field**[2], **M.D. Gray**[2], **V. Migenes**[3,*], **R.J. Cohen**[3], **and R.S. Booth**[4]

[1] Department of Physics, University of Bristol, Bristol BS8 1TL, UK
[2] School of Chemistry, University of Bristol, Cantock's Close, Bristol BS8 1TS, UK
[3] NRAL Jodrell Bank, University of Manchester, Macclesfield SK11 9DL, UK
[4] Onsala Space Observatory, S-43900 Onsala, Sweden

Received April 19, accepted June 8, 1993

Abstract. Results are reported from 5-station intercontinental VLBI observations of 1720 MHz OH masers in W3(OH). Two regions of maser emission were detected, superimposed on northern and southern parts of the H II region. Maser spots are individually unresolved and are ≤ 1.2 mas FWHM, placing an upper limit on interstellar scattering. These observations show that 1720 MHz maser spots are significantly smaller than 1665 MHz spots. Using a maser model described in Gray et al. (1992), the data are analyzed in terms of an accelerating and outflowing zone in the northern region, where 1720, 4765 and 1665 MHz maser spots may be spatially coincident. Geometrical effects leading to maser beaming in a turbulent medium are also modelled and these effects are sufficient to explain the relative sizes of maser spots at 1720 and 1665 MHz.

Key words: masers – techniques: interferometric – ISM: individual objects: W3(OH) – ISM: molecules – radio lines: interstellar

1. Introduction

Recent work has shown that masers can be successfully used as a probe of the physical conditions in massive star-forming regions (Cesaroni & Walmsley 1991; Gray et al. 1991; Gray et al. 1992, hereafter Paper I). In particular, detailed information can be obtained from the analysis of intense maser spots characterised using VLBI (e.g. Bloemhof et al. 1992 and references in Paper I). In the present work we report VLBI observations of 1720 MHz maser emission from the well-studied star-forming region W3(OH). Although 1720 MHz masers have been studied previously in several sources (e.g. Gaume & Mutel 1987; Fouquet & Reid 1982), 1720 MHz maser spot sizes have not previously been measured. Spot sizes are however a valuable diagnostic of maser beaming, provided interstellar scattering is not significant. An important motivation for the present observations was to test the hypothesis that 1720 MHz maser spots may be of smaller angular size than 1665 MHz spots. 1665 MHz maser spots have been studied in detail with VLBI as described in Bloemhof et al. (1992), Garcia-Barreto et al. (1988) and Reid et al. (1980) and we therefore have an extensive data set with which to compare our present work.

Our observational results are reported in Sects. 3 and 4. In Sect. 5 the 1720 MHz VLBI data, in conjunction with other data at 4765 and 1665 MHz, are analyzed to obtain the physical conditions in the outflowing zone in the northern part of W3(OH). This is essentially a reexamination of this region, originally treated in Paper I, in the light of the new observations presented here. In Sect. 6 we present a model for geometrical beaming of 1720 and 1665 MHz masers. We note that the angular size of maser spots may be fixed not only by morphological constraints, leading to "geometrical beaming", but also by self-beaming in saturated masers. We consider only geometrical beaming in the present work.

2. Observations and data reduction

Observations were made of 1720 MHz OH masers towards W3(OH), in November 1989 for a period of 12 h. The VLBI array consisted of five telescopes: Effelsberg (100 m), Onsala (25 m), NRAO Greenbank (43 m), Pietown (25 m) and Shanghai (25 m). Figure 1 shows the (u, v)-coverage and Fig. 2 the effective beam of the array. Observations were made using left-hand circular polarization and recorded using the standard MKII system with a bandwidth of 125 kHz. The observing frequency was set up to centre the emission in the band at a frequency of 1720.76 MHz, corresponding to a velocity relative to the LSR of -44 km s^{-1}. Half-hour scans on BL Lac, 3C84, NRAO150 and 2134 + 004 were interspersed throughout the observations to determine the bandpass calibration. The data were correlated using

Send offprint requests to: M.R.W. Masheder
* Present address: CSIRO Office of Space Science and Applications, ANU Campus, PO Box 3023, GPO Canberra, ACT2601, Australia

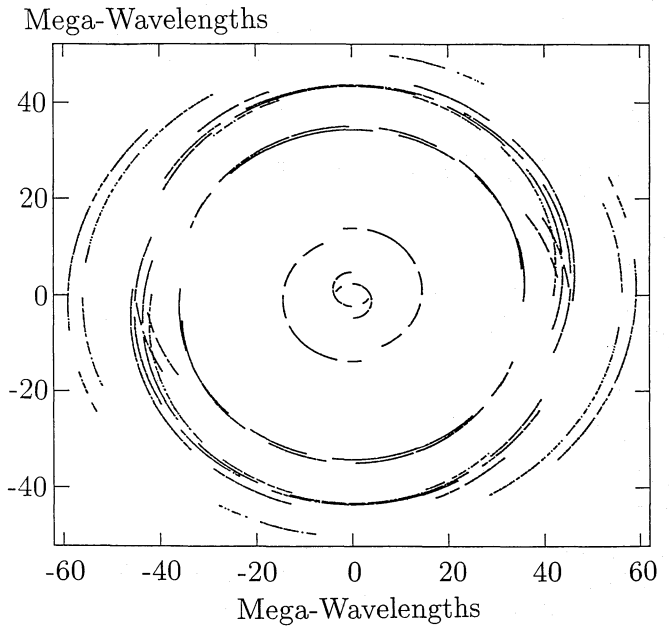

Fig. 1. The (u, v)-coverage obtained for W3(OH) from the 10 baselines formed from the 5 antennae used in the present observations. The quantities u and v are values, in megawavelengths, of the distance between antennae as seen from the source in the east and north directions, projected onto the disk of the Earth

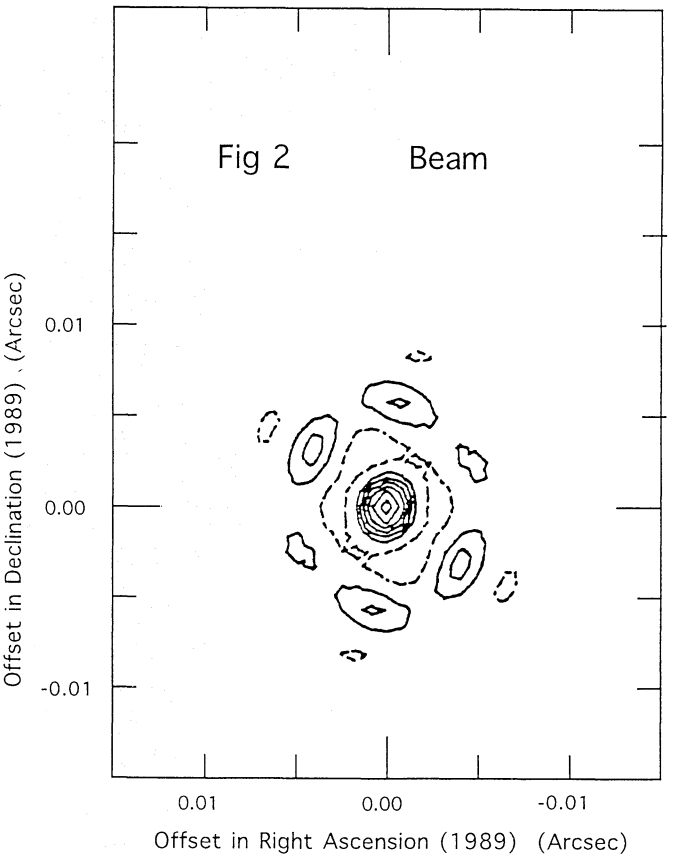

Fig. 2. The response of the VLBI interferometer to a point source (the "dirty beam") for the (u, v)-coverage shown in Fig. 1. Contour levels are at every 15% of the peak response. Dashed contours represent negative values

the MkII correlator, at the Max Planck Institut für Radioastronomie, Bonn, which generated 128 channels with a velocity spacing of 0.17 km s^{-1}. Hanning smoothing was used and so the effective velocity resolution in our experiment was 0.34 km s^{-1} (FWHM).

The correlated data were transported to AIPS for calibration and analysis. The calibration consisted of a bandpass correction (BPASS), a correction for antenna based Doppler shifts (CVEL), a determination of the flux density scale and fringe fitting. The amplitude calibration, for each source, was performed by creating a template spectrum based on the total power spectrum of the most sensitive antenna (Effelsberg 100 m). The template was then used to determine the amplitude scale for all the other antennae (ACFIT). Subsequent reduction and analysis of the data were performed using standard tasks.

After self-calibration using the feature at -45.5 km s^{-1}, maps were made from the channels that exhibited maser emission, using all baselines. Initially low resolution maps were made of a field covering 2.″4 by 2.″4, using a taper which de-emphasized the longer baselines. This revealed two regions of maser emission. These were then mapped individually with a narrower beam. The final maps of each region were 1024 × 1024 pixels in size, with cell-size of 0.8 mas and were "cleaned" with a restoring beam of 2.4 mas. The rms noise in the maps was $\sim$ 25 mJy. Here and throughout we use single polarization flux densities. Size estimates of maser features were determined from two dimensional gaussian fits to the maser spots and by fitting gaussian models to the (u, v) data, which gave the same results. Because of systematic effects in the maps due to limited u, v coverage, we only considered maser features brighter than 0.5 Jy. The procedure used allowed us to make an estimate of the absolute position of maser features to within about 0.″1.

3. Results

The two regions of 1720 MHz maser emission in W3(OH), mentioned in Sect. 2, are shown superimposed on a 15 GHz radio continuum map of the ultracompact H II region (dashed contours) in Fig. 3. The positional alignment is discussed in Sect. 4. The southern region is displaced from the northern region by $-0.''152$ in RA and $-1.''15$ in Dec.

Figure 4c shows the 1720 MHz total power spectrum in both lefthand circularly polarized (lhc; dashed lines) and righthand circularly polarized (rhc) recorded at NRAL Jodrell Bank in November 1989. Figure 5 shows channel maps of the northern and southern 1720 MHz features. The northern object (Fig. 5a–e) was found to be resolved by the interferometer and exhibits several features clustered within $\sim$ 15 mas. Individual maser spots within the group appear however to be unresolved. It should be noted that map c,

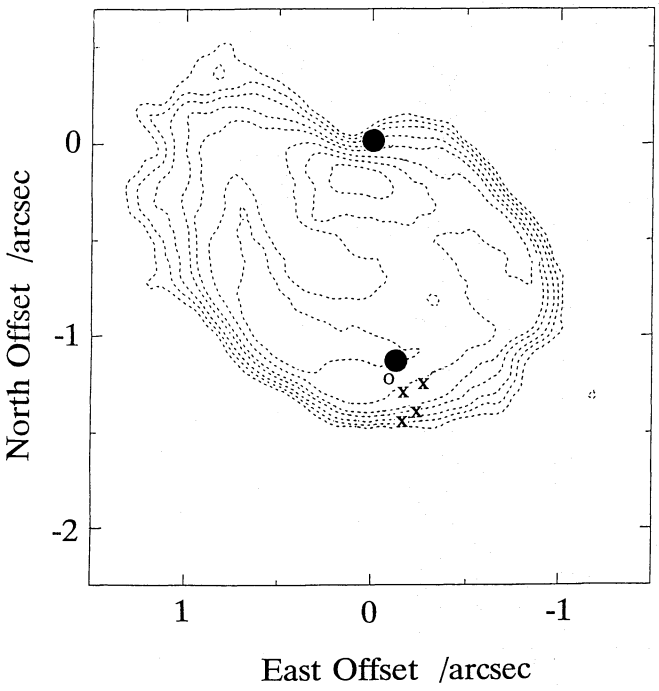

Fig. 3. Positions of 1720 MHz masers (•) (present observations), the 1665 MHz maser or maser cluster (○) nearest to the southern 1720 MHz maser zone (Garcia-Barreto et al.; Bloemhof et al.) and 4765 MHz masers (×) (Baudry et al.; Baudry and Diamond) superimposed on the 15 GHz radio continuum map of the ultracompact H II region in W3(OH) (from Masson 1989, private communication). The positions adopted for these maser spots are discussed in Sect. 4.2. At the position of the northern 1720 MHz maser zone, there may be a 1665 MHz maser cluster and a 4765 MHz maser zone (not shown), see text Sect. 4.2. The map origin is RA $02^h23^m16^s.47 \pm 0^s.01$, Dec.$61°38'57''.74 \pm 0''.1$ (1950)

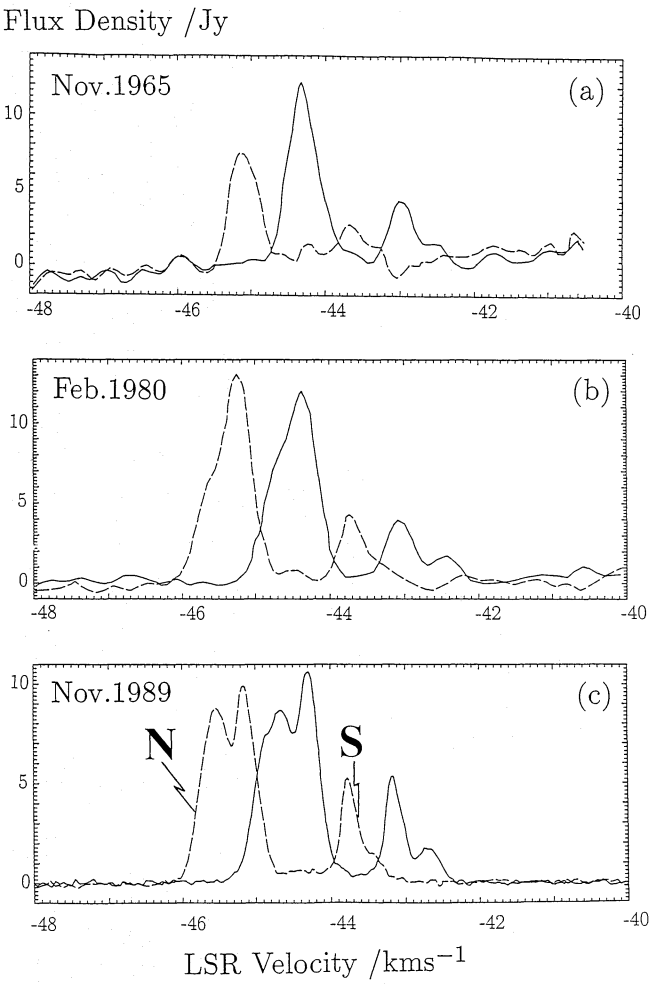

Fig. 4a–c. 1720 MHz total power spectra of W3(OH) taken at three different epochs: **a** Barrett & Rogers 1966, **b** Fouquet & Reid 1982, **c** this work. The frequency resolutions are respectively 0.22, 0.15 and 0.05 km s^{-1}. The dates shown on the spectra are the dates at which the spectra were recorded. Each spectrum has been digitized and redrawn on the same scale for direct comparison. Dashed lines correspond to lhc and solid lines to rhc. Intensity variations are discussed in Sect. 4.1. The symbols N and S in **c** identify the emission which is associated with the northern and southern maser zones. Note that the velocity scale in the data of Barrett & Rogers has been corrected to a rest frequency of 1720.530 MHz

and possibly map b, contain weak features which may be attributed to the dirty beam response, combined with the effects of calibration errors. Turning to the smaller, southern source, Fig. 5f, this was entirely unresolved in all channels, on the longest baseline in the system. Unresolved spots, in both the northern and southern regions have angular sizes of ≤ 1.2 mas, yielding linear sizes of $\leq 3.9\,10^{11}$ m, given a distance to W3(OH) of 2.2 kpc (Humphreys 1978). This spot size implies a peak brightness temperature of $8\,10^{11}$ K for a 1 Jy maser.

In Fig. 6a, b, c we have plotted flux versus velocity, in Fig. 6a and c integrating the flux over the total emission in the northern and southern regions respectively and, in Fig. 6b, over the two major features in the northern spot, so far as possible separately. In Fig. 6b, the higher negative velocity peak to the SW, with a maximum flux at -45.53 km s^{-1}, may be clearly identified with the high negative velocity component of the doublet in the lhc spectrum in Fig. 4c, at -45.59 km s^{-1}. The maximum in the NE component appears, however, to be displaced from the lower negative velocity component of this doublet by -0.17 km s^{-1}. From the velocity of the spectrum of the southern source in Fig. 6c, it is evident that the southern source may be identified with the feature at $\simeq$ 43.8 km s^{-1} in the total power spectrum of Fig. 4c. For the northern region, within observational error, all the flux at 1720 MHz was contained in the maser spots. In the southern region, about half the flux was detected. This is due to time averaging of the data with a possible small contribution from extended emission.

The most striking outcome of our observations is that 1720 MHz maser spots in W3(OH) are ~ 3 times smaller in linear size than the smallest 1665 MHz spots, which are 3 mas as recorded in Garcia-Barreto et al. (1988). This has

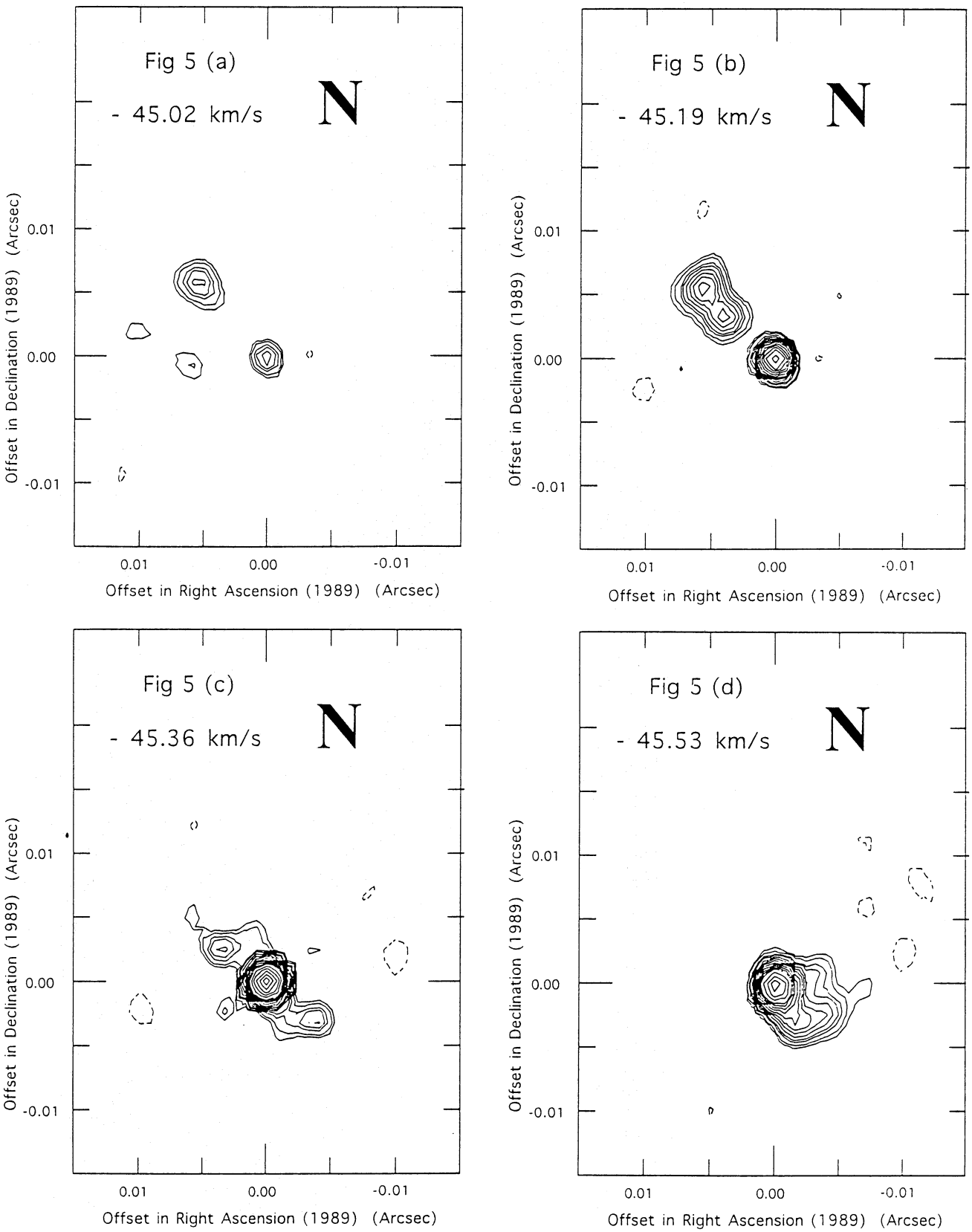

Fig. 5a–f. Selected channel maps of the maser zone in the northern region (**a–e**), and in the southern region (**f**). Each axis is labelled in arcseconds offset from the map origin. The position of the origin is RA $02^h23^m16^s.46 \pm 0^s.01$, Dec.$61°38'57''.8 \pm 0''.1$ (1950). Contour levels (/Jy) are 0.25, 0.3, 0.375, 0.425, 0.5, 0.575, 0.65, 0.75, 0.875, 1.0, 1.13, 1.25, 1.5, 1.75, 2.0, 2.25, 2.5, 2.75, 3.0. The restoring beam was 2.4 mas in diameter (FWHM)

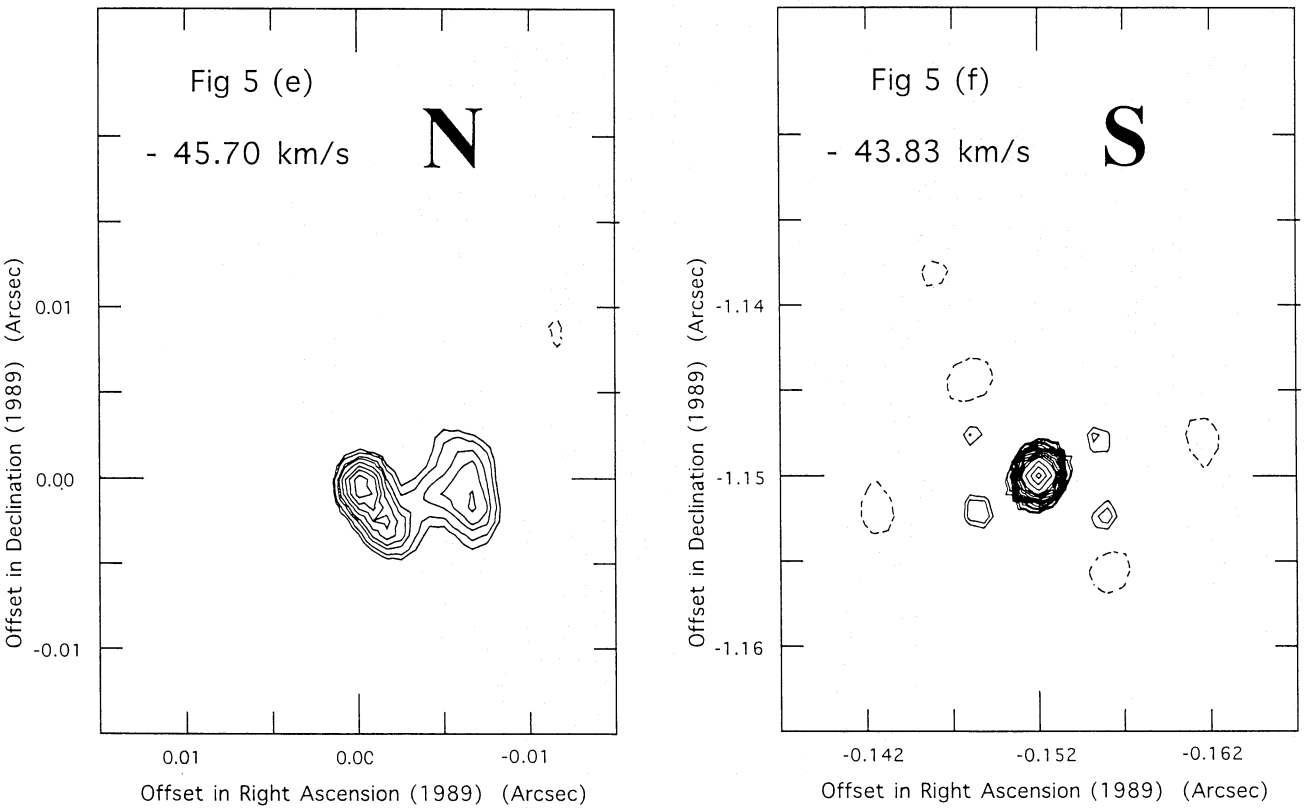

Fig. 5 (continued)

interesting consequences for the gas dynamics in the maser zone, as we see in Sect. 6.

4. Discussion of results

This section is divided into (i) a discussion of the 1720 MHz total power spectrum in Fig. 4c, with reference to spectra taken at earlier epochs, Fig. 4a and b, (ii) the detailed spatial association of 1720 MHz maser spots with those at 1665 and 4765 MHz and (iii) a brief comparison with recent methanol maser data.

4.1. 1720 MHz total power spectra: intensity variations

Our spectra show the close match between lhc and rhc lineshapes, as observed in earlier work, Fig. 4a (Barrett & Rogers 1966) and 4b (Fouquet & Reid 1982). Comparison with previous spectra shows that a high negative velocity feature, associated with the northern region, has grown into both lhc and rhc spectra since 1965, the date of the Barrett & Rogers observations. We resolve two clear peaks of similar flux at higher negative velocity and Fouquet & Reid see a weaker feature appearing as a shoulder, whereas the feature is altogether absent in Barrett & Rogers. The emergence of this new feature is also clear from the FWHM of our double peak, of $0.87\,\mathrm{km\,s^{-1}}$, compared with the single peaked feature of Barrett & Rogers with FWHM of $0.47\,\mathrm{km\,s^{-1}}$. Turning to the lower negative velocity feature, associated with the southern region, the flux in this velocity range remained ~ 0.33 of that of the higher negative velocity feature between 1965 and 1980 (the date of the Fouquet & Reid observations). Since that date, however, the relative flux in this feature has grown to ~ 0.52 of the higher velocity feature.

4.2. The spatial association and velocities of 1720, 4765 and 1665 MHz maser spots

We identify our bright northern maser spot with the single 1720 MHz VLBI spot measured by Fouquet and Reid, at the same velocity. The absolute positional accuracy of their measurements was $0''.1$, similar to the present data (see Sect. 2). However Fouquet and Reid measured the relative positions of 1720 and 1665 MHz with an accuracy 30 mas. This shows that our bright northern spot is closely spatially coincident with a group of high flux 1665 MHz masers, in the vicinity of the map origin at RA $02^{h}23^{m}16^{s}.47 \pm 0^{s}.01$, Dec. $61°38'57''.74 \pm 0''.1$ (1950). This cluster has an average demagnetized velocity of $-46.3\,\mathrm{km\,s^{-1}}$ (Bloemhof et al. 1992) where the averaging extends over a range of ≤ 60 mas. The separation of the lhc and rhc peaks in Fig. 4c, for the northern 1720 MHz feature, suggests a

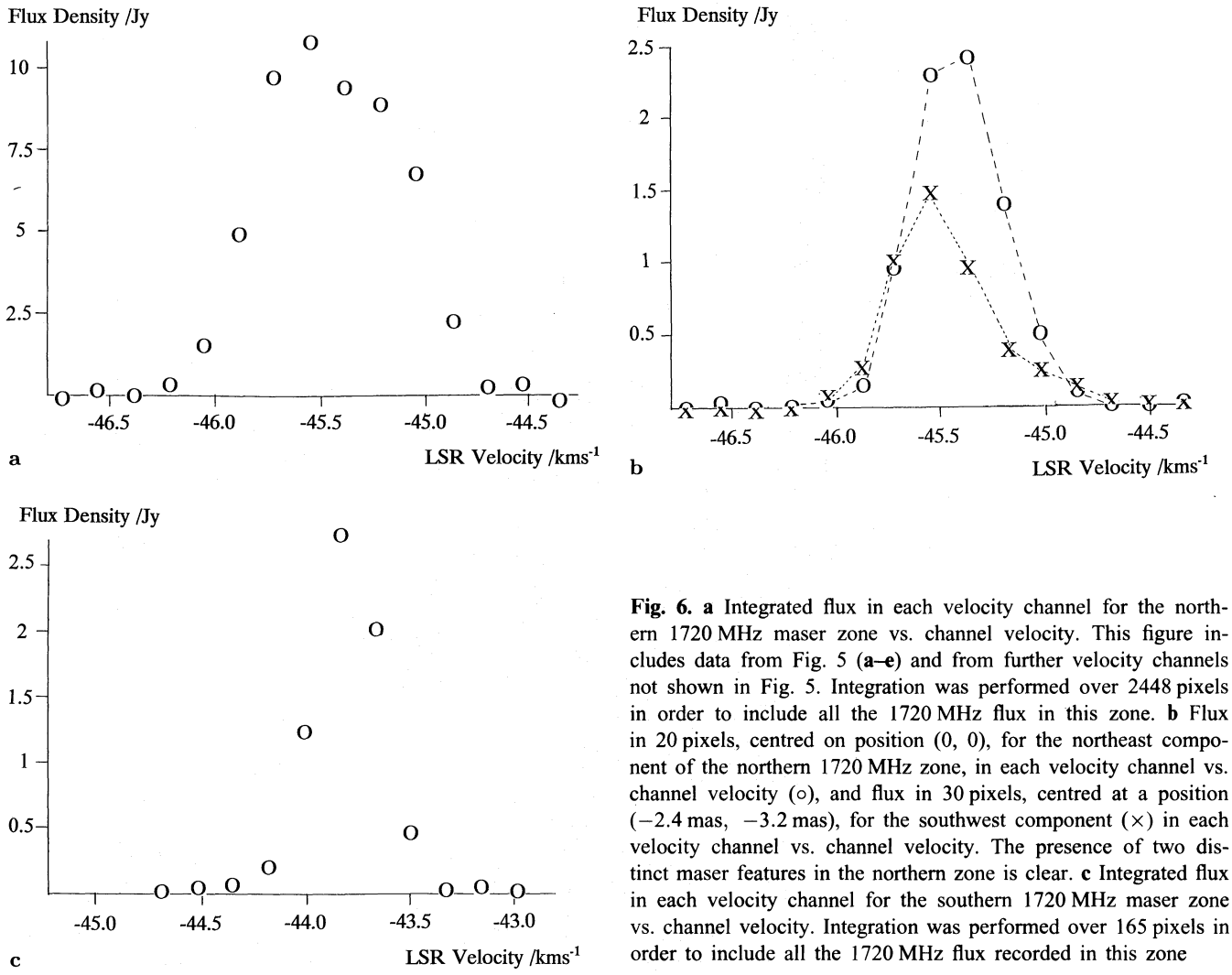

Fig. 6. a Integrated flux in each velocity channel for the northern 1720 MHz maser zone vs. channel velocity. This figure includes data from Fig. 5 (**a–e**) and from further velocity channels not shown in Fig. 5. Integration was performed over 2448 pixels in order to include all the 1720 MHz flux in this zone. **b** Flux in 20 pixels, centred on position (0, 0), for the northeast component of the northern 1720 MHz zone, in each velocity channel vs. channel velocity (○), and flux in 30 pixels, centred at a position (−2.4 mas, −3.2 mas), for the southwest component (×) in each velocity channel vs. channel velocity. The presence of two distinct maser features in the northern zone is clear. **c** Integrated flux in each velocity channel for the southern 1720 MHz maser zone vs. channel velocity. Integration was performed over 165 pixels in order to include all the 1720 MHz flux recorded in this zone

magnetic field of 8.1 ± 0.1 mG, given a shift of 0.055 km s^{-1} mG^{-1} for 1720 MHz. Bloemhof et al. record a field of 8.2 mG for their -46.3 km s^{-1} 1665 mHz maser cluster. With regard to the southern source, this was not detected by Fouquet & Reid.

Turning to 4765 MHz emission, we adopt the assumption, introduced by Baudry et al. (1988) and Baudry & Diamond (1991), that 4765 MHz emission, in their region A, is spatially superimposed on the northern 1720 MHz maser zone, itself superimposed on either the -46.3 km s^{-1} 1665 MHz cluster or the -45.55 km s^{-1} maser spot. This spatial superposition of maser spots at different frequencies is essentially a working hypothesis, which cannot be justified by the absolute positional accuracy of the measurements. In the case of these 4765 MHz VLBI observations, the absolute positional accuracy may be in doubt by as much as 1 arcsecond.

In Paper I it was shown that, by considering the spatial and velocity relationship of masers at 1720, 1665 and 4765 MHz, it was possible to provide a semi-quantitative description of the physical conditions and dynamics in the maser zone. Our present data demand a reappraisal of that analysis, since we now have detailed spatial and velocity information at 1720 MHz. Specifically our new data show that 1720 and 4765 MHz maser features do not overlap in velocity and must therefore be formed in distinct parts of the medium. The distribution of flux in the velocity channels of the 4765 and 1720 MHz data is shown in Fig. 7. This demonstrates that the assumption made in Paper I, that the 1720 MHz emission extended from demagnetised velocities of -42.4 to -45.0 km s^{-1}, was incorrect. As we show in Sect. 5, this has important consequences for the physical conditions which we derive for this region.

Given the spatial superposition of 4765, 1720 and 1665 MHz in the northern region, we find that these three frequencies are not spatially superposed within observational error in the southern region. Masers at these three frequencies are however closely associated, since a 1665 MHz cluster (Bloemhof et al. 1992), or a single maser spot (Garcia-Barreto et al. 1988), lie within ~ 60 mas and

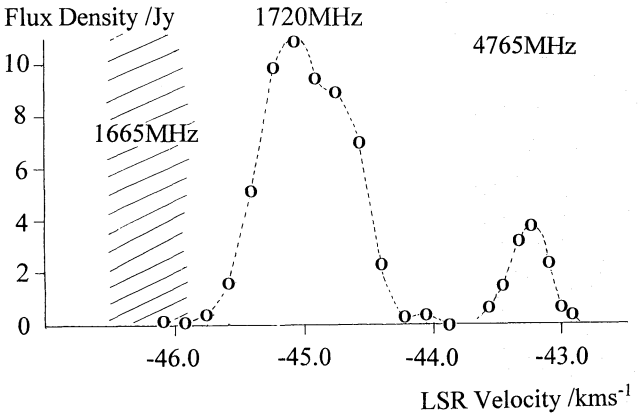

Fig. 7. Bulk, demagnetized velocities of 4765, 1720 and 1665 MHz features in the northern zone in W3(OH), represented by the integrated flux vs. velocity channel for 1720 MHz, as in Fig. 6a, and for 4765 MHz (taken from Baudry et al., region A). Velocities of the 1720 MHz line have been demagnetized using a field of 8.1 mG (see Sect. 4.2). The 1665 MHz maser cluster is schematically represented with an average, demagnetized velocity of $-46.3\ \mathrm{km\,s^{-1}}$ (Bloemhof et al.)

4765 MHz (region B in Baudry et al. 1988) within 100 to 200 mas of the southern 1720 MHz maser spot. This is illustrated in Fig. 3. Evidently the southern region is an active zone, but the three frequencies do not emanate from the same column of gas, always assuming the superposition in the northern region.

4.3. Association with methanol masers

Recent observations of methanol masers (Menten et al. 1992) show that there are two especially active regions at 6.7 and 12.2 GHz: an extended northern region and a compact southern region separated by about $-0''.08$ in RA and $-1''.16$ in Dec. The absolute positions of these regions agree with those of our 1720 MHz masers, within the experimental accuracy of $0''.1$, established through comparison with Fouquet and Reid. However, there is not a one-to-one correspondence of features, reflecting the different source structures in the northern region, the methanol distribution being considerably more extended. Nevertheless, there appears to be a clear association between sites active at 1720 MHz and methanol at 6.7 and 12.2 GHz.

5. An analysis of the physical conditions in the northern region

We seek to identify the physical conditions which may lead to the spatial superposition of 4765, 1720 and 1665 MHz as suggested in Sect. 4.2. In order to determine these conditions we use a model of the maser environment, described in detail in Gray et al. (1991), coupled with a many-level semiclassical theory of maser propagation (Field & Gray 1988). FIR line overlap, involving lines connecting levels of different J, is included in our analysis (Doel et al. 1990). The consequence of overlap is that we predict a sequence of masers in an accelerating flow, with 4765 MHz in a hot dense region, with 1720 MHz further along the flow, and with 1665 MHz in the coolest and least dense zone.

We treat the northern region, on the largest scale (that is, greater than any turbulent scale) as an adiabatically expanding flow, accelerating, cooling and dropping in number density as expansion progresses, as in Paper I but now with modified physical conditions. We assume a velocity field of $5000\ \mathrm{km\,s^{-1}\,pc^{-1}}$. A significant departure from Paper I arises because our present observations require that we identify initial and low velocity shift conditions which create 4765 MHz maser action in the *absence* of 1720 MHz, since we find that 1720 MHz and 4765 MHz do not overlap in velocity. It turns out that 4765 MHz masers form, in the absence of other masers, at high number densities and high OH concentrations, with no dust present in the maser zone itself. We initiate the outflow at a kinetic temperature of 250 K and a number density of $10^8\ \mathrm{cm^{-3}}$, five times higher than in Paper I, with an external dust component at 250 K spatially diluted by a factor of 16. The initial flow velocity is set at $0.5\ \mathrm{km\,s^{-1}}$, the thermal velocity. The physical conditions change along the expanding flow according to number density = initial number density $\times 0.5/(0.5+\Delta v)$ and kinetic temperature = initial kinetic temperature $\times\{0.5/(0.5+\Delta v)\}^{-2/3}$, where Δv is the velocity shift in $\mathrm{km\,s^{-1}}$ introduced by adiabatic expansion. We allow gain lengths to decrease from an initial value of $3.5\ 10^{12}$ m to a final value of $< 5\ 10^{11}$ m. We find that 4765 MHz is the only strong maser present up to shifts of 0.3 to $0.4\ \mathrm{km\,s^{-1}}$. Beyond this shift, with number density $\leq 5\ 10^7\ \mathrm{cm^{-3}}$ and kinetic temperature ≤ 160 K, 1720 MHz rapidly dominates achieving a maximum flux around a shift of $0.7\ \mathrm{km\,s^{-1}}$. At the same time, 4765 MHz drops to a negligible intensity. For $\Delta v > 0.6\ \mathrm{km\,s^{-1}}$, the model flow enters a zone containing dust at the kinetic temperature. Progressing further along the flow, 1720 MHz decays and at shifts of $\geq 2\ \mathrm{km\,s^{-1}}$, with a kinetic temperature between 90 and 100 K and a number density of $2\ 10^7\ \mathrm{cm^{-3}}$, 1665 MHz becomes the dominant maser. The full length of the flow, up to the $-46.3\ \mathrm{km\,s^{-1}}$ 1665 MHz zone, as in Paper I is $2.3\ 10^{13}$ m, calculated from the velocity shift and the assumed velocity field.

Our analysis clearly yields the correct qualitative behaviour, with the initial independent emergence of 4765 MHz, followed by 1720 MHz and then by 1665 MHz as we progress along the flow. In Fig. 8a we show the results of calculations for 196 K, $6.9\ 10^7\ \mathrm{cm^{-3}}$, shift = $0.22\ \mathrm{km\,s^{-1}}$, in Fig. 8b for 110 K, $2.9\ 10^7\ \mathrm{cm^{-3}}$, shift = $1.22\ \mathrm{km\,s^{-1}}$, and in Fig. 8c for 73 K, $1.6\ 10^7\ \mathrm{cm^{-3}}$, shift = $2.67\ \mathrm{km\,s^{-1}}$, showing results representative of the three sets of conditions which yield 4765, 1720 and 1665 MHz respectively. As we noted in Paper I, our model contains many approximations which preclude an accurate analysis and we find in the present work that the observed and calculated

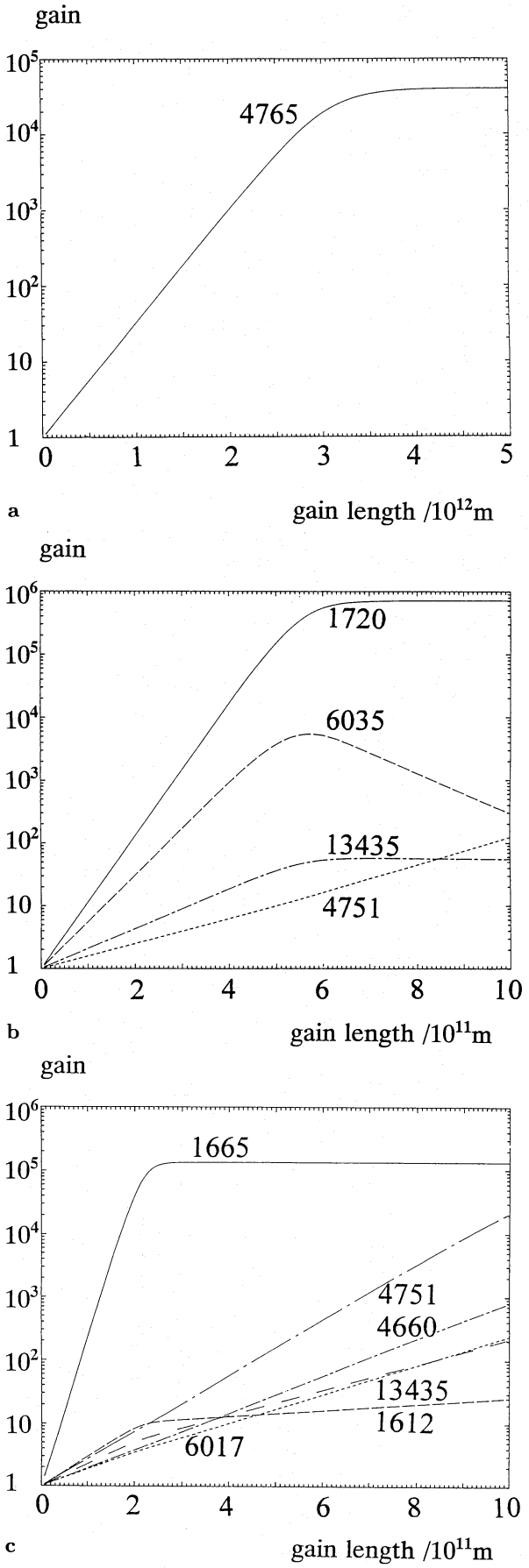

velocities are not in good agreement, with the 1720 MHz zone predicted to occur at an insufficiently negative velocity (by $\sim 0.7\ \mathrm{km\,s^{-1}}$).

Our suggestion of an accelerating flowing zone is consistent with observations of Bloemhof et al. and the general association of masers with shocks produced by an expanding H II region (Elitzur & de Jong 1978; Hartquist & Sternberg 1991). The H II region may have encountered the edge of its parent molecular cloud in the northern part of W3(OH) with the molecular gas undergoing adiabatic expansion into the low pressure intercloud medium. A shock preceding the ionization front may destroy the dust in its immediate vicinity, through heating to > 1000 K (Hartquist & Sternberg), yielding the warm dust-free, dense and OH-rich environment of the 4765 MHz maser. The dust either reforms in the expelled gas or is expelled ahead of the shock, yielding the 1720 and 1665 MHz maser zones.

6. Geometrical beaming of the 1720 MHz masers

Our observations show that 1720 MHz maser spots in W3(OH) are smaller in angular size than those at 1665 MHz. Data of Garcia-Barreto et al. (1988) and Reid et al. (1980) together record a variety of 1665 MHz spot sizes ranging from 3 to 14 mas with an average value of ~ 5 mas, whereas our results give ≤ 1.2 mas for 1720 MHz. The calculations described in Sect. 5 show that the distance traversed by a maser ray for saturation of 1720 MHz is typically a factor of 3 times greater than for 1665 MHz, for conditions favouring either 1720 or 1665 MHz exclusively. This result is valid over a wide range of physical conditions and is illustrated in Fig. 8b, c. In this section we set out to compute the relationship between spot size and gain length, assuming that the spot size is determined by the geometrical distribution of amplifying material. We do not consider the contribution to beaming due to saturation. We also assume that the upper limit on the spot size of 1720 MHz masers represents the upper limit on the physical dimensions of the maser face in the plane of the sky, and is not significantly influenced by interstellar scattering.

We expect the maser zone to be turbulent (Moran et al. 1978; Field 1982; Scalo 1987), with several discrete regions along the line-of-sight contributing to maser gain. Such regions might be eddies at closely similar Doppler velocities, which by chance line up and provide a path of amplification. Such eddies are not however readily identifiable in

Fig. 8. **a** Maser growth as a function of gain length for $T = 196$ K, H_2 number density $= 6.9\,10^7\ \mathrm{cm^{-3}}$, velocity shift $= 0.22\ \mathrm{km\,s^{-1}}$, showing the emergence of 4765 MHz as the sole masing transition. **b** As for **a** but with $T = 110$ K, H_2 number density $= 2.9\,10^7\ \mathrm{cm^{-3}}$, velocity shift $= 1.22\ \mathrm{km\,s^{-1}}$, showing the emergence of 1720 MHz as the sole strong maser **c** As for **a** but with $T = 73$ K, H_2 number density $= 1.6\,10^7\ \mathrm{cm^{-3}}$, velocity shift $= 2.67\ \mathrm{km\,s^{-1}}$, showing the emergence of 1665 MHz as the sole strong maser

maps. Evidently the projected area in the plane of the sky, over which such regions overlap, decreases as the number of such regions increases. Hence the requirement for longer gain lengths for 1720 MHz, as compared with 1665 MHz, would in this model result in 1720 MHz masers appearing of smaller angular size on purely geometrical grounds – hence the expression "geometrical beaming". We now investigate this quantitatively.

We use a model of the maser zone, with conditions suitable for the formation of either 1720 or 1665 MHz, composed of turbulent gas, in which are embedded regions, numbering between 12 and $1.25\,10^4$, at the same Doppler velocity and therefore capable of yielding amplification at a common line-centre frequency. We adopt a Monte-Carlo technique by which we introduce these regions at random positions within the maser zone. For simplicity, all regions are taken to be spherical. We have performed separate calculations for a range of different sized regions (see below). In this preliminary study, we make no distinction between media which support 1720 or 1665 MHz masers, nor do we attempt to introduce velocity shifts explicitly into the model. The volume filling factor of gas, able to amplify a maser ray, and the characteristic size of a region relative to the total extent of the maser zone, are input parameters. We consider randomly directed lines-of-sight through such a zone. Computation proceeds, for each line-of-sight, by determining the number of regions along this line-of-sight. Lines-of-sight are classified according to the number of regions traversed within the maser zone. For each such classified path, we then calculate its angular extent by varying the direction of the ray until the number of regions traversed changes. This is repeated for five variations of direction to obtain an average angular extent. We encounter paths with increasing numbers of regions with rapidly decreasing probability, as we record in Table 1. For each type of path we sum the averaged angular extents and average once more over the total number of paths of that type. We adopt a volume filling factor of 0.1 throughout our calculations. Turbulence commands all scales of amplifying regions. We have therefore used the maximum useful range of characteristic region sizes, encompassing maser amplification extending from very weak amplification to strong saturation. Our calculations show that this involves a factor of 10 in gain length. We choose the size of the largest region to be 0.2 times the total size of the maser zone, where this upper limit is chosen to avoid a single dominant region. We then average our calculated values of solid angle, for each type of path, over the range of region sizes, weighting the average according to a Kolmogorov-type scaling such that the number of regions is proportional to (region size)$^{-4/5}$ (Scalo 1987). Our final averaged values of solid angle for each type of path are shown in Table 1.

Table 1. The results of the analysis described in Sect. 6, where n is the number of regions traversed by a maser beam, N_n is the average number of lines-of-sight associated with traversing n regions and Ω_n is the corresponding average solid angle in which maser beams are contained

Number of regions n	Lines-of-sight N_n	Solid angle Ω_n/sr
1	2462 ± 49	$3.50 \pm 0.03\ 10^{-2}$
2	1591 ± 39	$1.12 \pm 0.01\ 10^{-2}$
3	1010 ± 31	$3.01 \pm 0.04\ 10^{-3}$
4	611 ± 21	$1.20 \pm 0.02\ 10^{-3}$
5	369 ± 15	$1.10 \pm 0.02\ 10^{-3}$
6	179 ± 10	$2.06 \pm 0.05\ 10^{-4}$
7	76 ± 6	$8.2 \pm 0.3\ 10^{-5}$
8	37 ± 4	$2.1 \pm 0.1\ 10^{-5}$
9	13 ± 2	$1.75 \pm 0.15\ 10^{-5}$
10	5 ± 1	$2.4 \pm 0.3\ 10^{-5}$

Since 1720 MHz requires typically 3 times the gain length of 1665 MHz to yield strong saturated amplification, 1720 MHz maser rays therefore traverse three times as many regions, on average, as 1665 MHz maser rays. The ratio of the angular sizes, of 1665 and 1720 MHz spots is therefore given by the ratio $(\Omega_n/\Omega_{3n})^{1/2}$, where Ω_n is the solid angle associated with the path involving n regions. For $n = 1$, 2 and 3, ratios of linear size are respectively 3.4 ± 0.05, 7.4 ± 0.1 and 13 ± 0.5. These ratios scale approximately linearly with the chosen volume filling factor. For a value of 0.1, given a 1720 MHz maser spot size of ≤ 1.2 mas, effects of geometrical beaming therefore yield a prediction of 1665 MHz maser spot sizes in the range $\leq 4.1 \pm 0.05$, $\leq 8.9 \pm 0.1$ and $\leq 15.5 \pm 0.7$ mas, reproducing the observed range of 1665 MHz spot sizes, noting that in each case ($n = 1$, 2 or 3) an arbitrary scaling factor, for the physical size of the maser zone, may be introduced. This suggests that 1665 MHz masers with 3 to 4 mas spot sizes form by amplification through a single region, those between 5 and 8 mas, by amplification through two regions, and those between 9 and 14 mas, by amplification through three regions. The apparent contradiction, with the trend of beam angle in Table 1, comes about because of the requirements of constant gain length and constant filling factor. We note that the 1665 MHz maser at -45.5 km s^{-1}, in the northern zone, is of angular size 4 mas (Garcia-Barreto et al. 1988) and we therefore find that, in this zone, the 1720 MHz maser amplifies by traversing three regions and the 1665 MHz maser by traversing one region.

We now consider the relative likelihood of encountering $n = 1$, 2 or 3 region paths and compare our predictions with observations of the relative prevalence of 1665 MHz masers of various angular size. For this purpose we have computed the number of paths involving n regions, N_n, using weighted averages with Kolmogorov scaling, as used for the values of solid angle. Values of N_n are shown in Table 1. Values of N_1/N_2 and N_2/N_3 should reproduce the relative prevalence of 1665 MHz masers, respectively of sizes 3 to 4 mas and 5 to 8 mas, and 5 to 8 mas and 9 to 14 mas. Using the data of Garcia-Barreto et al., noting that the data of

Reid et al. give essentially the same result, we find that the observed relative prevalence of 3 to 4 mas masers and 5 to 8 mas masers is 1.36 ± 0.01. The computed value, N_1/N_2, is 1.54 ± 0.07. The observed relative prevalence of 5 to 8 mas masers and 9 to 14 mas masers is 2.3 ± 0.3 and the calculated value 1.6 ± 0.1. Considering the simplicity of the model, this is satisfactory agreement. Turning to the relative prevalence of 1665 and 1720 MHz masers, results in Paper I show that 1665 MHz may form over a larger range of physical parameters compared to that for 1720 MHz. Therefore considerations only of paths, as here, might be expected to give an upper bound to the relative prevalence of 1720 MHz masers. Our observations and those of Garcia-Barreto et al. show that the number of 1665 MHz spots is 10 to 15 times the number of 1720 MHz spots. Values of N_n in Table 1 allow us to assign probabilities, P_n, of traversing n regions yielding $P_1 = 0.39 \pm 0.02$, $P_2 = 0.25 \pm 0.01$, $P_3 = 0.16 \pm 0.01$, $P_6 = 0.028 \pm 0.002$ and $P_9 = 0.002 \pm 0.0002$. Hence the relative chance of encountering paths traversing 1, 2 or 3 regions compared with 3, 6 or 9 regions, that is, the relative occurrence of 1665 and 1720 MHz masers, is given by $P_1 + P_2 + P_3/(P_3 + P_6 + P_9)$. This has the value of 4.2 ± 0.5, as a limiting value, in accord with the above discussion.

We consider now the values of flux at the telescope which our computed maser beam angles and factors of amplification suggest. We consider as examples the 1720 and 1665 MHz maser spots in the northern region, with respectively ~ 10 and ~ 40 Jy flux. For 1720 MHz, in Fig. 8b for example, we find a saturated amplification factor of $7\,10^5$, where we amplify the black-body background at the kinetic temperature of the medium, 110 K (see Paper I). The flux at the output face of the maser, I_M, is therefore $7\,10^{-14}$ Wm^{-2} Hz^{-1}. This is related to the observed flux, I_{obs}, by $I_{obs} = I_M(\Omega_S/\Omega_M)$ where Ω_S is the measured spot size in steradians and Ω_M is the maser beam angle, geometrical values of which we have estimated above (Table 1). For 1720 MHz maser spots our observations show that $\Omega_S \leq 2.2\,10^{-17}$ sr. Thus, in order to record a flux of 10 Jy, we require that Ω_M be $\leq 1.6\,10^{-5}$sr. A similar analysis for 1665 MHz shows that, in order to record a flux of 40 Jy, Ω_M must $\leq 10^{-5}$ sr, using the amplification factor in Fig. 8c and a value of Ω_S corresponding to 4 mas. These figures are similar to those derived in Paper I. We note that the inclusion of complete velocity redistribution may increase values of Ω_M by a factor of ~ 3 (Gray et al. 1993; Field et al. 1993). Geometrical beaming in 1720 MHz in the northern region yields $\Omega_M = 3\,10^{-3}$ sr, corresponding to traversal of 3 regions (see Table 1). For 1665 MHz the figure is $3.5\,10^{-2}$ sr, for 1 region. This leads to the conclusion that geometrical beaming alone cannot in general account for the very small maser beam angles that theory and observation together appear to dictate. Self-beaming due to saturation must be invoked to reduce the maser beam angle by a further 2 to 3 orders of magnitude. In this connection it is interesting to note that, if 1720 MHz maser rays traversed 9 regions, then geometrical beaming would alone be sufficient to reproduce the observed flux.

7. Concluding remarks

The first VLBI measurement of 1720 MHz spot sizes is reported. These spots turn out to be significantly more compact than those measured at 1665 MHz. This can be understood in terms of a simple model of geometrical beaming. The observation of 1720 MHz maser spots of ≤ 1.2 mas FWHM has the consequence that interstellar scattering must contribute less than this figure in W3(OH). Hence the present results show that the resolved angular sizes of 1665 MHz maser spots, as recorded in previous publications, are true spot sizes and should no longer be regarded as upper limits on the true spot size.

The analyses presented in Sects. 5 and 6 have shown how VLBI observations can give considerable insight into the nature of the OH maser zone in massive star-forming regions. Observational evidence as a whole, coupled with detailed maser modelling, shows that masers in H II regions form over a range of conditions from $\leq 10^8$ H$_2$ cm^{-3} to $< 10^7$ cm^{-3}, from $T = 250$ to < 50 K, with or without dust in the maser zone, in accelerating, outward directed flows. Maser propagation takes place through amplification along randomly directed lines-of-sight within a turbulent medium, which, in the standard picture (Elitzur & de Jong 1978; Shu 1991), is being driven outwards by an expanding H II region.

Our techniques of analysis however remain rather primitive and the present work serves to highlight the shortcomings of both observation and theory. With regard to observation, phase referencing, for precise comparison of positions of maser spots at different frequencies, is now available on the VLBA and on MERLIN. Future observations, planned on both these installations, will establish the spatial relationship of maser spots, at different frequencies, to within a few mas. This will remove a major source of uncertainty in analyses such as that presented in Sect. 5. Present results also show that truly intercontinental baselines are required to resolve spots at 1720 MHz.

Acknowledgements. We should like to thank the Directors and Staff of the telescopes involved in this project and in particular we thank D. Graham, W. Sherwood and W. Alef (MPI für Radioastronomie, Bonn) for extensive help in correlating the VLBI data. We also thank P. Diamond (NRAO) and J. Yates (Jodrell Bank) for help with AIPS. We should also like to express our thanks to A.E.E Rogers for sending us copies of his thesis and a technical report relating to the 1965 observations of 1720 MHz maser emission. We are grateful to the SERC for PDRA support for MDG and to the Royal Society for the award of a 1983 University Research Fellowship to MDG.

References

Barrett A.H., Rogers A.E.E., 1966, Nat 210, 188
Baudry A., Diamond P.J., 1991, A&A 247, 551

Baudry A., Diamond P.J., Booth R.S., Graham D., Walmsley C.M., 1988, A&A 201, 105
Bloemhof E.E., Reid M.J., Moran J.M., 1992, ApJ 397, 500
Cesaroni R., Walmsley C.M., 1991, A&A 241, 537
Doel R.C., Gray M.D., Field D., 1990, MNRAS 244, 504
Elitzur M., 1990, ApJ 363, 638
Elitzur M., de Jong T., 1978, A&A 67, 232
Field D., 1982, MNRAS 201, 527
Field D., Gray M.D., 1988, MNRAS 234, 353
Field D., Gray M.D., de St. Paer P., 1993, A&A (to appear)
Fouquet J.E., Reid M.J., 1982, AJ 87, 691
Garcia-Barreto J.A., Burke B.F., Reid M.J., Moran J.M., Haschick A.D., Schilizzi R.T., 1988, ApJ 326, 954
Gaume R.A., Mutel R.L., 1987, ApJS 65, 193
Gray M.D., Doel R.C., Field D., 1991, MNRAS 252, 30
Gray M.D., Field D., Doel R.C., 1992, A&A 262, 555 (Paper I)
Gray M.D., Jones K.N., Field D., 1993, J.C.S. Farad. Soc. 89, 2231
Hartquist T.W., Sternberg A., 1991, MNRAS 248, 48
Humphreys R., 1978, ApJS 38, 309
Menten K.M., Reid M.J., Pratap P., Moran J.M., 1992, ApJ 401, L39
Moran J.M., Reid M.J., Lada C., Yen Y.L., Johnston K.J., Spencer J.H., 1978, ApJ 224, L67
Reid M.J., Haschick A.D., Burke B.F., Moran J.M., Johnston K.J., Swenson G.W., 1980, ApJ 239, 89
Scalo J.M., 1987, in: Hollenbach D.J., Thronson H.A. (eds.) Interstellar Processes, Proc., Astrophysics and Space Science Library, Reidel, Dordrecht, p. 349
Shu F.H., 1991, The Physics of Astrophysics, Vol. II, Gas Dynamics. University Science Books, California, ISBN 0-935702-65-2